ADVANCED MATERIALS
www.advmat.de

Fully 3D-Printed Miniature Soft Hydraulic Actuators with Shape Memory Effect for Morphing and Manipulation

Haitao Qing, Yinding Chi, Yaoye Hong, Yao Zhao, Fangjie Qi, Yanbin Li, and Jie Yin*

Miniature shape-morphing soft actuators driven by external stimuli and fluidic pressure hold great promise in morphing matter and small-scale soft robotics. However, it remains challenging to achieve both rich shape morphing and shape locking in a fast and controlled way due to the limitations of actuation reversibility and fabrication. Here, fully 3D-printed, sub-millimeter thin-plate-like miniature soft hydraulic actuators with shape memory effect (SME) for programable fast shape morphing and shape locking, are reported. It combines commercial high-resolution multi-material 3D printing of stiff memory polymers (SMPs) and soft elastomers and direct printing of microfluidic channels and 2D/3D channel networks embedded in elastomers in a single print run. Leveraging spatial patterning of hybrid compositions and expansion heterogeneity of microfluidic channel networks for versatile hydraulically actuated shape morphing, including circular, wavy, helical, saddle, and warping shapes with various curvatures, are demonstrated. The morphed shapes can be temporarily locked and recover to their original planar forms repeatedly by activating SME of the SMPs. Utilizing the fast shape morphing and locking in the miniature actuators, their potential applications in non-invasive manipulation of small-scale objects and fragile living organisms, multimodal entanglement grasping, and energy-saving manipulators, are demonstrated.

1. Introduction

Miniature soft actuators at millimeter or smaller scales[1] have the intrinsic small-size advantages to operate in confined spaces, making them suitable for broad potential applications in delicate grasping, drug delivery, and medical diagnosis.[2–4] Generally, the actuation mechanisms for shape morphing in miniature soft actuators can be classified into two main categories:[1,4,5] one is based on external stimuli-responsive soft materials, such as various soft active actuators in response to solvent, electricity, heat, light, and magnetic field.[6,7] The other is based on fluidic pressure-driven elastomers such as pneumatic or hydraulic soft actuators with patterned fluidic channels embedded in elastomers.[8,9] Both stimuli-responsive and fluidic shape mechanisms have their advantages and disadvantages in terms of fabrication, actuation response, and control.[1,4,5] For example, stimuli-responsive soft materials can be easily processed into thin sheets and small sizes for intricate 2D-to-3D shape morphing[10,11] and robotic applications.[11,12] However, controlling the shape-morphing actuation is nontrivial, since it is challenging to program in-plane or cross-thickness inhomogeneous expansion/contraction embedded in soft active materials for target out-of-plane deformation in a controlled fashion.[13,14] In contrast, the fluidic actuation, widely used in the soft robotics community, facilitates fast and reversible actuation responses, easy fabrication, and simple control.[8,9,15] In addition to simple bilayer bending widely used for soft robotic manipulation, fluidic actuation also enables the generation of similar complex 2D-to-3D shape morphing to soft active materials but in a more facile and controllable way, e.g., by programing the anisotropic deformation of the networked air channels embedded in homogenous soft pneumatic actuators.[16]

Despite the promise of fluidic actuation, several challenges remain that hinder its broad applications in miniature soft robotics and morphing matter in terms of fabrication and actuation.[1,4] First, miniaturizing the conventional bulky macroscale soft fluidic actuators to light-weight planar forms with submillimeter thickness, similar to thin sheet-based stimuli-responsive soft actuators[10] remains challenging[4] The challenge resides in the facile fabrication of microfluidic channels embedded in thin-layered soft elastomers in terms of both high resolution and complexity in networked channels[16] The traditional molding method is limited to the fabrication of millimeter-scale channels.[8,9,15,16] Despite the recent advances in high-solution fabrication techniques of microfluidic soft actuators using soft lithography[17] and 3D printing,[18–20] they are often costly and require either complicated multi-step microfabrication or carefully tailored materials formulation and processing.[18–20]

H. Qing, Y. Chi, Y. Hong, Y. Zhao, F. Qi, Y. Li, J. Yin
Department of Mechanical and Aerospace Engineering
North Carolina State University
Raleigh, NC 27695, USA
E-mail: jyin8@ncsu.edu

The ORCID identification number(s) for the author(s) of this article can be found under https://doi.org/10.1002/adma.202402517

DOI: 10.1002/adma.202402517

Second, given their fully reversible actuation responses, most stimuli-responsive and fluidic soft actuators are energy inefficient[5] especially for robotic manipulation and shape-morphing applications since they need to consume additional energy to hold the grasped objects or retain the morphed shapes.[10] Among all the soft actuation materials, heat or light-responsive shape memory polymers (SMPs) provide unique characteristics of shape memory effect (SME) for shape programing, locking, and recovering.[21,22] SMPs can be programed and locked into a temporary shape under loading at a temperature beyond the glass transition temperature (T_g) followed by cooling and unloading. Consequently, after re-heating above T_g, they can recover to their original permanent shape. Recent studies show the promise of embodying SME in various soft active materials such as liquid crystal elastomer and magneto-responsive elastomer or composites for programable shape shifting and shape locking.[23–25] However, it remains largely unexplored, concerning integrating SME with miniature soft hydraulic actuators for programable fast shape morphing, shape locking, and shape recovery in a simple and controlled manner, as well as energy-efficient and noninvasive manipulation.

In this work, we propose fully 3D-printed, thin-plate-like miniature soft hydraulic actuators (MSHAs) with SME for delicate and noninvasive manipulation, programable shape morphing, shape locking, and shape recovery (Figure 1). The miniature soft actuators have submillimeter thickness and are composed of a soft elastomer layer with embedded microfluidic channels and a strain-limit stiff SMP layer (Figure 1a). The MSHAs are directly printed in a single print run via the PolyJet printing method using commercial multi-material 3D printers (i.e., Stratasys Objet 260 Connex 3 3D Printer, Figure S1, Supporting Information). The microfluidic channel is directly printed by replacing solid support materials with non-curing fluid[26] in high resolution (Figure 1a). This eliminates the time-consuming and challenging step of dissolving support materials inside the confined spaces of microfluidic channels in conventional 3D printing.[27] Consequently, it opens new avenues in enabling the efficient and high-resolution printing of simple or complex microfluidic networks embedded in a thin elastomeric sheet. Meanwhile, the multi-material 3D printing enables the direct printing of layered or patterned soft-hard composites with SME in a controllable and programable manner (Figure 1b). Thus, it allows for programing microfluidic channel networks and/or multi-materials distribution in a thin sheet for reversible, controllable, and versatile fast actuated 2D-to-3D shape morphing, as well as shape locking and recovery by utilizing the SME (Figure 1c). We demonstrate the proof-of-concept applications of such programable fast miniature soft actuators as noninvasive and delicate soft grippers capable of grasping a living ant and a human hair, and multimodal tendril-like soft manipulators, as well as energy-efficient soft grippers by utilizing the SME to lock their grasped shapes.

2. Results

2.1. Design of Miniature Soft Hydraulic Actuators for Shape Morphing and Locking

Figure 1a(ii) shows the construction of a simple miniature soft hydraulic bending actuator. It is composed of two materials in a bilayer structure: a stiff layer of SMP and a soft layer of elastomer with an embedded straight microfluidic channel. At room temperature, the SMP layer acts as a strain-limit layer since its modulus (glassy state, ≈1 GPa) is three orders higher than the elastomer (≈1 MPa) (See details in Figure S2, Supporting Information). The elastomer layer acts as the hydraulic actuation layer upon fluid infusion, which drives the bending of the actuator. The actuator can be printed in high resolution (digital material build mode ≈30 µm) via the PolyJet printing method. The cross section of the microfluidic channels can go down to 200 µm (width) × 200 µm (height) and the layer thickness can be as thin as 100 µm for successful and repeated hydraulic actuation. The thickness of the 3D-printed miniature soft actuator can be down to the sub-millimeter scale, as shown in the example of a ≈500 µm-thick actuator in Figure 1a(iii).

The bended shape can be temporarily locked and recover to its initial flat shape repeatedly utilizing the SME (Figure 1b). At the actuated bended state, when remotely heating the SMP layer under infrared (IR) light above T_g, the SMP layer soft-ens with comparable modulus to the elastomer. The tempo-rary bended shape can be locked upon rapidly cooling below T_g. In this way, any programed actuated shape can be locked for either fixing the morphed shape or holding grasped ob-jects without consuming additional energy. It can recover to its permanent original flat shape upon reheating above T_g (Figure 1b).

The direct printing of microfluidic channels alongside the high-resolution multi-material printing in flat layered configurations offers potentially tremendous design space for rich programmed 2D-to-3D actuated shape morphing and related robotic applications. The fast and controllable shape morphing and shape locking can be achieved by programing the structured multi-materials and/or patterning of the microfluidic channel networks. For example, in the single-channel bending actuator (Figure 1c(i)), replacing the uniform SMP layer (SMP and elastomer are highlighted in light orange and blue color, respectively) with patterned oblique SMP segments leads to a distinct tendril-like actuator, which curls and twists upon actuation for potential entanglement grasping (Figure 1c(ii)). Furthermore, more complex microfluidic channel networks can be directly printed and embedded in the elastomer layer for target 2D-to-3D shape morphing, for example, an actuated warping leaf-like shape with similar branched vein patterns as the channel network (Figure 1c(iii)) that can be locked and recovered. Next, we will discuss and showcase the potential of the fully 3D-printed thin plate-like MSHAs for shape morphing/locking and versatile object manipulations.

2.2. Miniature Soft Hydraulic Bending Actuators

Figure 2a–c shows the hydraulic-driven bending of the simple miniature soft bending actuator with a single straight microfluidic channel. The thin actuator has a sub-millimeter thickness h = 800 µm, length l = 20 mm, and width w = 3 mm. The top stiff SMP layer and the bottom elastomer layer have a thick-ness of h_l = 100 µm and h_m = 700 µm, respectively. The microfluidic channel takes a rectangular cross section of 300 µm (width) × 200 µm (depth). The microfluidic channel is infused

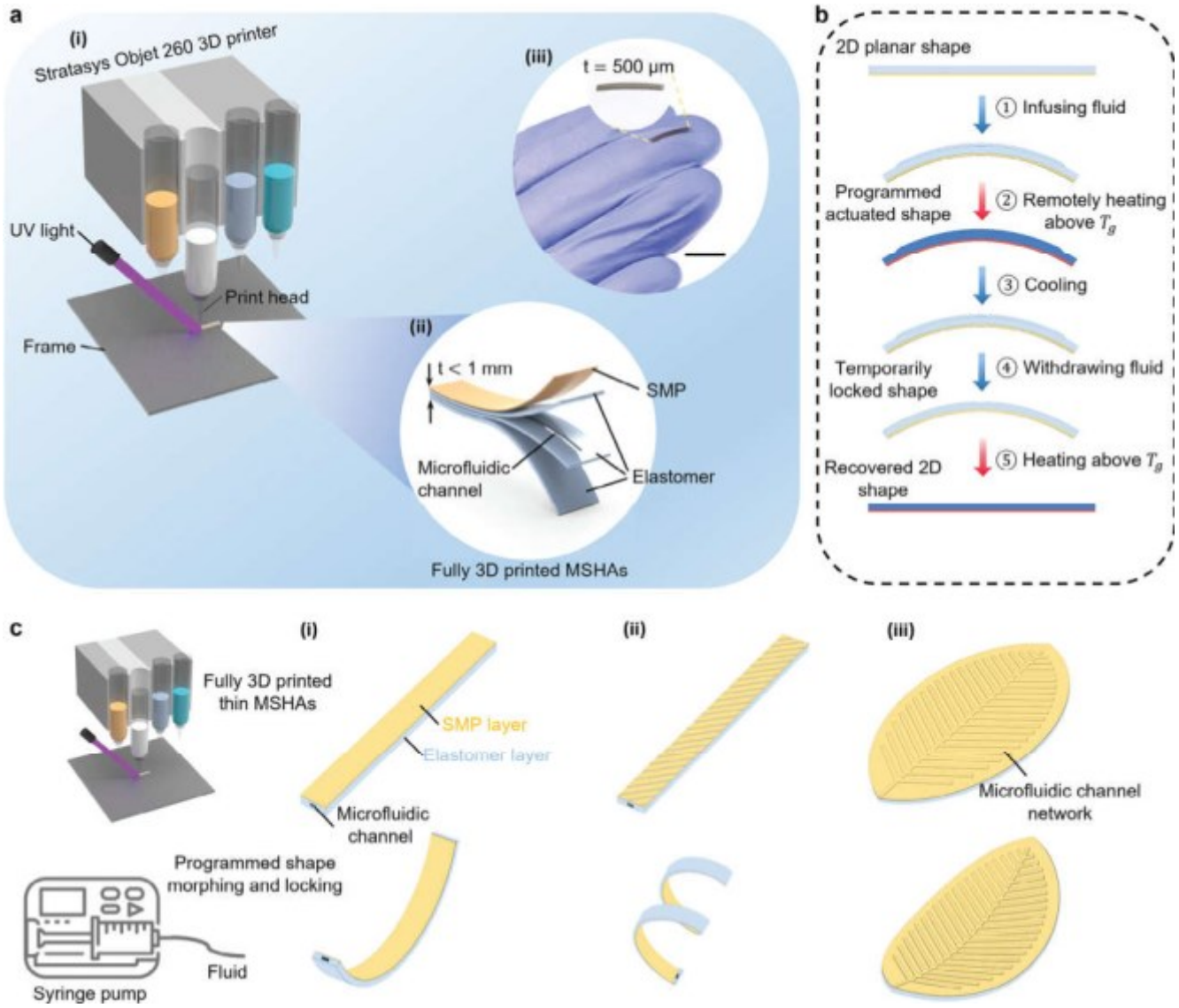

Figure 1. Schematic illustrations of the fully 3D-printed miniature sub-millimeter-thick soft hydraulic actuator (MSHA) integrated with the SME for shape morphing and shape locking. a) Schematics of fabricating the MSHA using a commercial multi-material 3D printer (i). The MSHA comprises a stiff SMP layer and a soft elastomer layer with a microfluidic channel printed inside using non-curing fluid (ii) (The thickness of all actuators is smaller than 1 mm). The inset shows the printed MSHA with thickness of 500 μm (iii). b) Schematics of the shape morphing, locking, and recovery processes by activating the SME in the MSHA in five steps. c) Schematic illustration of programed shape morphing/locking from thin planar configurations into circular, helical, and warping shapes in three example MSHAs by manipulating either the channel network or the patterning of multi-material printed hybrid compositions. (i) Straight beam with a uniform SMP layer. (ii) Straight beam with a patterned oblique SMP layer. (iii) Leaf-like MSHA with branched vein-like microfluidic channel networks.

with water using a syringe pump (see Experimental Section for details). This expands and hydraulically pressurizes the bottom elastomer layer, which drives the bending.

Figure 2a shows that upon the increase of infused fluid volume V, the miniature soft hydraulic actuator can gradually bend upward into a fully closed circle (Figure S3 and Movie S1, Supporting Information), which is well captured by the corresponding finite element method simulation (Figure 2b, see details in Experimental Section) and analytical modeling (Figure 2c). Further increase of V leads to a bending angle 휃 over 360° (Figure S4 and Movie S2, Supporting Information) without fracture, similar to the well-studied macroscopic soft fluidic bending actuators,[15,28] which is, however, over 2.5 times larger than the maximum bending angle (135°) in the reported 3D printed miniature soft pneumatic actuator due to the constituent printed materials failure[19] Compared to its macroscale counterparts,[15,28] it only requires over 250 times smaller volume to bend into a nearly closed ring (Figure 2a) due to its miniaturized size.

At a given V, a thicker stiff layer leads to a smaller 휃 (Figure 2d–f). The expansion of the elastomer layer yields the bending moment[29] which results in the bending of the actuator. Its bending curvature 휃 can be predicted via the simplified

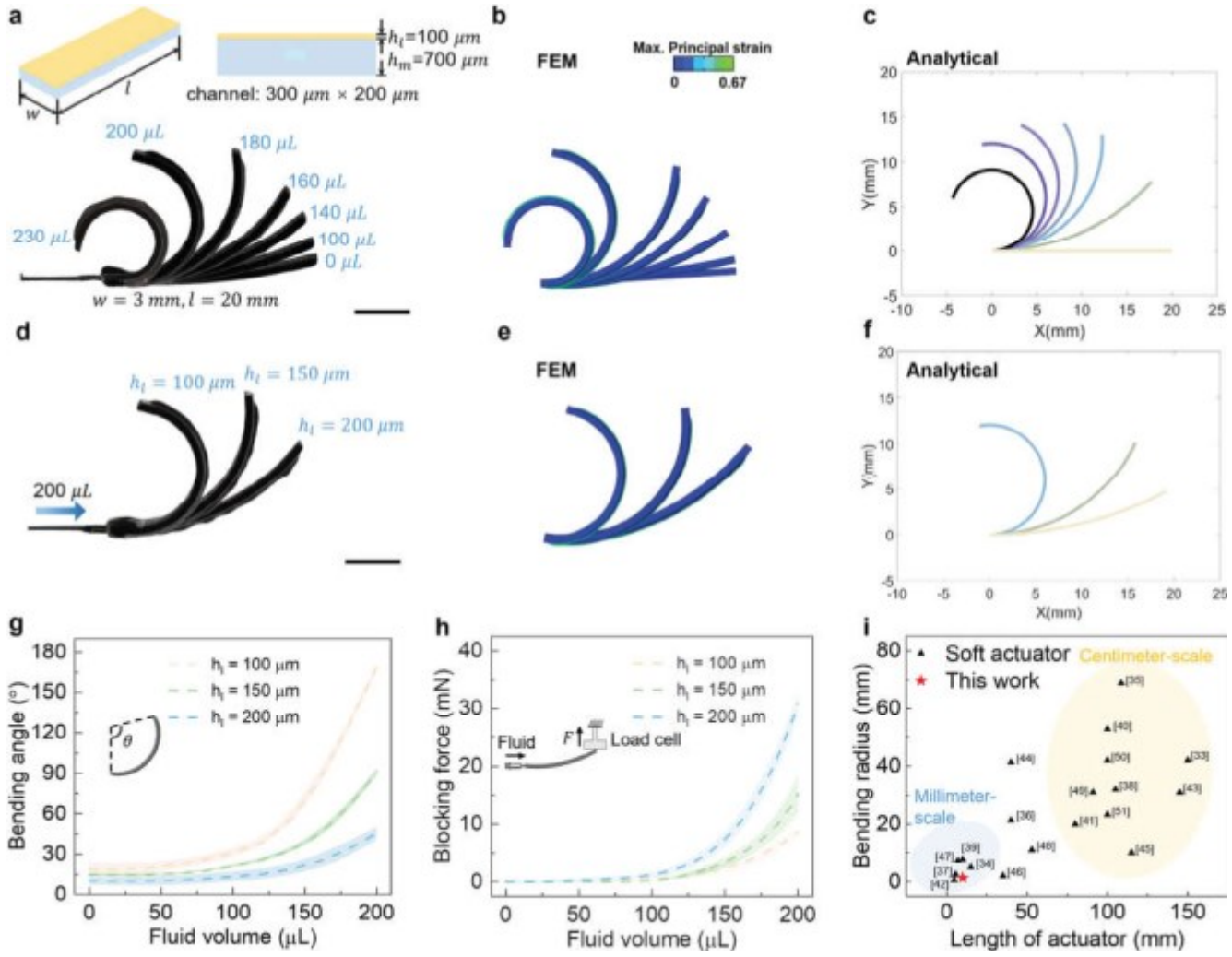

Figure 2. Miniature soft hydraulic bending actuators with large bending angle, small bending radius, and small blocking forces. a) Schematic illustration of the geometry and size of the single-channel actuator (top) and the snapshots of bending into a nearly closed circle in the printed sample upon fluid infusion from 0 μL to 230 μL (bottom). w = 3 mm, l = 20 mm, h_l = 100 μm (SMP layer), and h_m = 700 μm (elastomer layer). The microfluidic channel size is 300 μm × 200 μm. Scale bar: 5 mm. b,c) The corresponding FEM simulation and analytical result. d–f) Effect of top stiff layer thickness h_l on the bended shapes under the same infusing fluid volume of 200 μL through experiments (d), FEM simulation (e), and analytical modeling (f). Scale bar: 5 mm. g,h) Comparison of the bending angle (g) and blocking force (h) versus fluid volume for actuators with different h_l. The inset shows the schematics of blocking force measurement. i) Comparison of the bending radius versus the actuator length between this work and other reported soft bending actuators.[33–51] The blue and yellow circles highlight millimeter-scale and centimeter-scale soft actuators. Scale bar: 5 mm.

theoretical model (see details in Supporting Information), where 휃 is given by

$$휃 = \frac{E_m A \, V_e^n}{(1 - 휈^2) B_e^n V_0} \quad (1)$$

Where E_m and 휈 are the Young's modulus and Poisson's ratio of the elastomer layer, respectivley. A is the cross-section area of the microfluidic channel. l_e and B_e denote the effective offset distance due to the movement of neutral axis and the effective bending rigidity of the miniature actuator,[30] respectively. n denotes the nonlinearity factor describing how the compliance of the channel changes with volume[31] V and V_0 are the infused fluid volume and the initial volume of the microfluidic channel, respectively. The analytical solutions (Figure 2c,f) are consistent with both experiments (Figure 2a,d) and FEM simulation results (Figure 2b,e).

Figure 2g,h shows the actuated bending angle 휃 and the measured blocking force F as a function of infused fluid volume V and h_l varying from 100 μm to 200 μm (h_m = 700 μm is fixed), respectively. Both figures show that 휃 and F increase nonlinearly with V by following similar J-shaped curves. As expected, increasing h_l leads to a dramatically decreasing bending angle but increasing blocking force. The peak blocking forces are in the range of ≈8.7 – 30.8 mN, which is two orders smaller than its macroscale counterparts (the order of several newtons)[8,9,15,16] (Figure S5, Supporting Information). Such a small mN-scale blocking force is even lower than the reported stretching-driven ultra-gentle miniature kirigami gripper (≈35.5 mN)[32] that is capable of noninvasively grasping a fragile water drop and

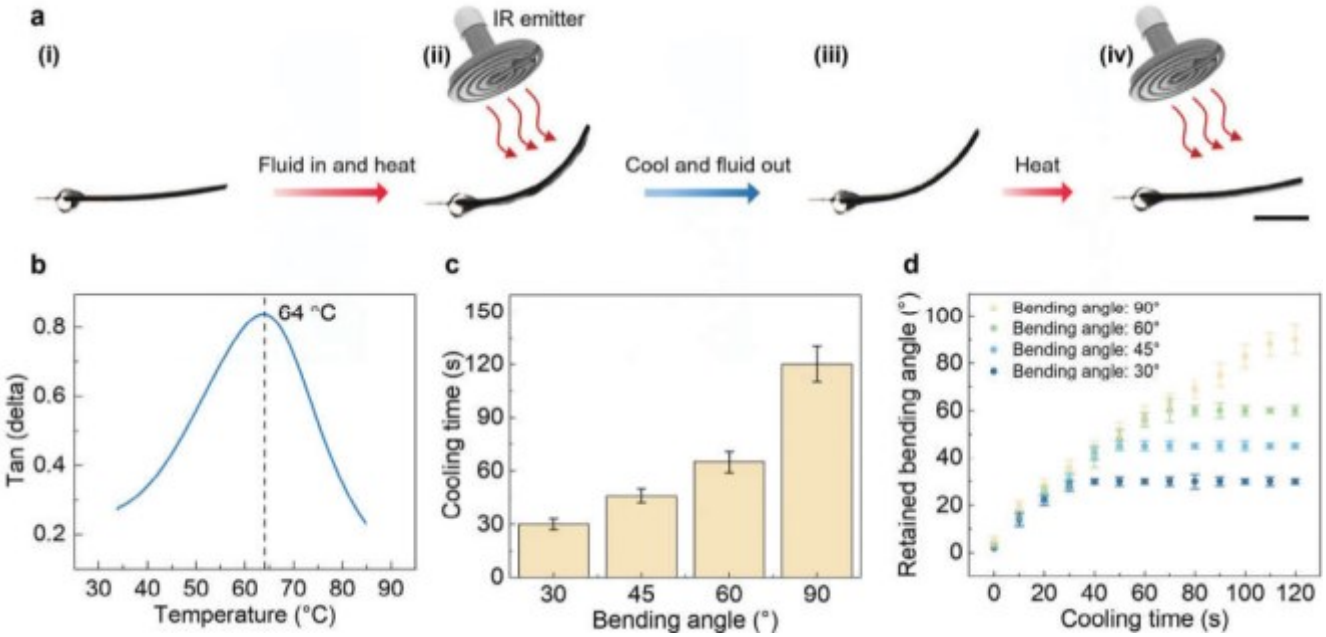

Figure 3. a) Actuation process of a 3D printed MSHA having SME. For the sake of enhancing the SME, the actuators in Figure 2 and Figure 5 are fabricated with a thicker SMP (thickness: 200 μm) compared to previous actuators. b) Thermomechanical property of SMP measured by Dynamic Mechanical Analysis (DMA). Tan delta as a function of the temperature. The dashed line indicates that the glass transition temperature of the SMP is 64 °C. c) Cooling time required for different locked bending angles of 30°, 45°, 60°, and 90°. d) Comparison of retained bending angle versus cool-ing time for bilayer MSHAs with different bending angles of 30°, 45°, 60°, and 90°. (Total thickness of each MSHA = 900 μm, l = 30 mm, h = 200 μm, h_m = 700 μm).

≈6–20 times smaller than the centimeter-scale, ultragentle soft hydraulic robotic gripper (≈0.2 N)[33] that can handle fragile jellyfishes. In addition to its small force, it also shows a small bending radius R, e.g., R ≈3.2 mm in Figure 2a. The smallest R can be less than 1 mm by reducing h (e.g., h = 500 μm shown in Figure 1a) and l (e.g., l = 10 mm shown in Movie S3, Supporting Information) which is smaller than other miniature soft bending actuators[34–40,42–51] and at least one order of smaller than the macroscale fluidic bending actuators (R > 1 cm) with millimeter-scale thickness and channel features fabricated by traditional molding/demolding approaches[15,28] (Figure 2i) (see details in Table S1, Supporting Information). Such mm-scale bending radius and mN-scale blocking force alongside large bending angles will facilitate delicate manipulation of small-scale objects in confined spaces as discussed later.

2.3. Integrating SME for Shape Locking

We explore utilizing the SME in the stiff SMP layer alongside direct printing for shape locking in the fully 3D-printed miniature soft hydraulic actuators. We start with examining activating the SME in the simple single-channel soft bending actuator discussed above for locking its actuated bended shape, as shown in Figure 3a. After the actuator bends to the desired bending angle under hydraulic pressurization, it is then exposed to a remote IR emitter for heating above T_g of the SMP (Figure 3a(ii)), meanwhile, the applied hydraulic pressure is retained to maintain its bended shape during heating. The T_g of the printed SMP is measured to be ≈64 °C (Figure 3b). Above T_g, the SMP becomes soft and has a modulus of ≈1 MPa (Figures S6 and S7, Supporting Information), three orders lower than the modulus at room temperature (≈1 GPa). Rapidly cooling the bended soft actuator to room temperature with the hydraulic pressurization retained can temporarily lock its deformed shape. After withdrawing the infused fluid, it can maintain the bended shape (Figure 3a(iii)). We note that to activate the SME, the thickness of the 3D-printed SMP layer should be at least 200 μm.

To evaluate the controllability of locking the MSHAs with SMPs, we further examine the cooling time t_{cool} required for locking the bended shapes under different locked bending angles, which are shown in Figure 3c. It shows that a longer cooling time is required to fully lock a larger bending angle. As the bending angle 휃 increases from 30° to 90°, t_{cool} increases from ≈30 s to ≈120 s. Figure 3d further compares the retained bending angle $휃_R$ versus the cooling time for the bilayer MSHAs. It shows that for any bending angle, the MSHAs will partially recover to its original flat configuration if the cooling time is insufficient to fully lock the MSHAs. Interestingly, the MSHAs with different bending angles follow the similar nonlinear $휃_R$-t_{cool} curve.

2.4. Programable Miniature Soft Hydraulic Bending Actuators

Beyond single-channel actuation, the fully 3D multi-material printed strategy can be applied to the multiple spatially interconnected microfluidic channels driven by a single hydraulic input, for example, the design of miniature flower-like soft bending actuators shown in Figure 4a and Figure S8 (Supporting Information). It is composed of a top stiff SMP layer, an elastomer layer

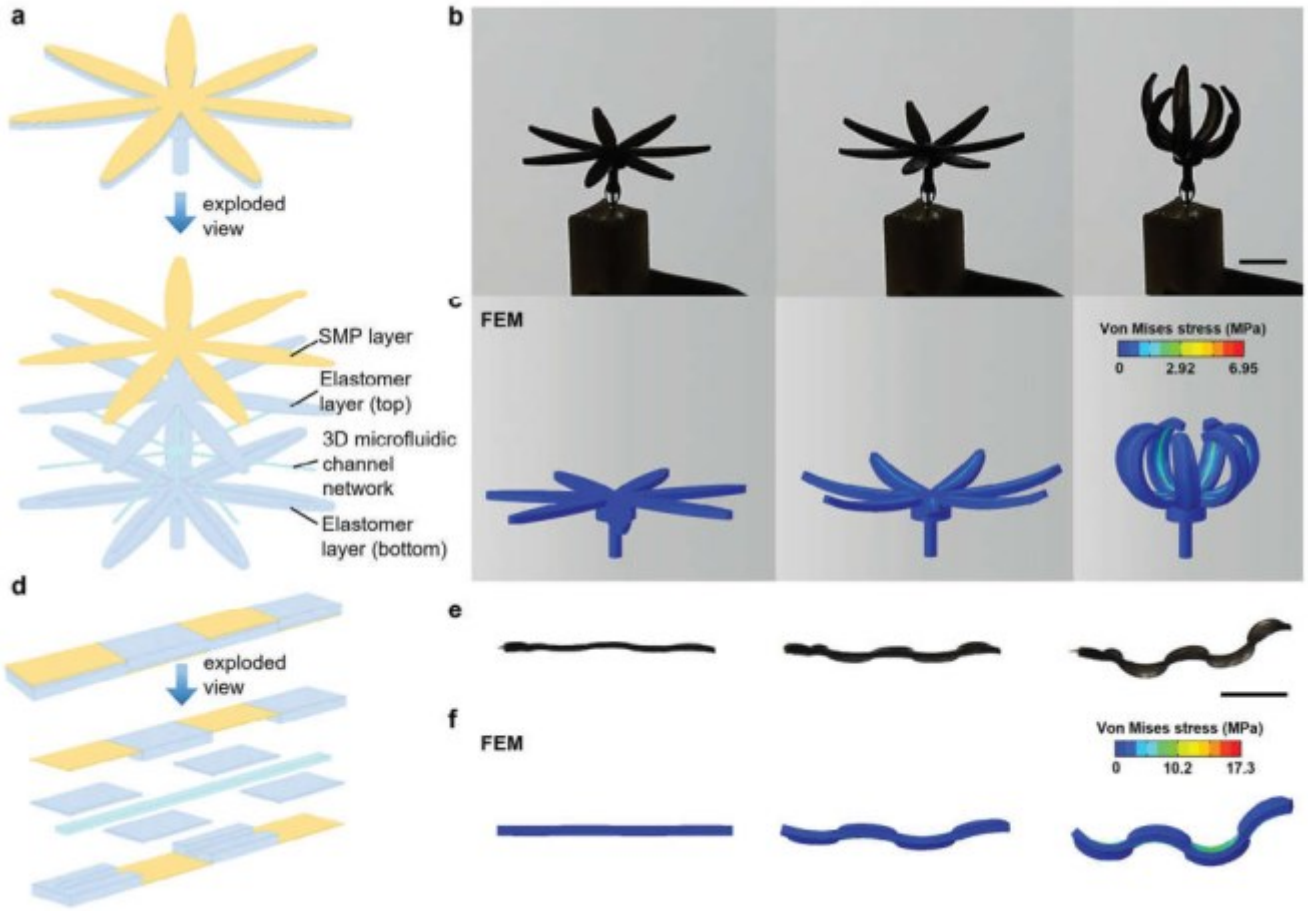

Figure 4. Programing directly 3D printed spatial microfluidic channel networks and/or hybrid patterning for actuated flower-like and wavy shapes. a) Schematics of a 3D miniature flower-like soft bending actuator with the exploded view of layered structures. b,c) Snapshots of a mimicking flower closing upon fluid infusion in experiments and corresponding FEM simulation. Scale bar: 10 mm. d) Schematic of a planar miniature segmented bending actuator with exploded view of layered structures. e,f) Snapshots of flat-to-wavy shape morphing upon fluid infusion in experiments and corresponding FEM simulation. Scale bar: 10 mm.

underneath with embedded star-shape-like microfluidic channels, and an elastomeric peduncle. The jointed lateral star-like channels in the pedals are connected to a vertical channel in the peduncle. This creates a 3D interconnected microfluidic channel network that is directly 3D-printed and actuated under single pressure. The microfluidic channel takes a rectangular cross section in the pedals, with dimensions of 400 µm (width) × 200 µm (depth), and a circular cross section in the peduncle, with a radius of 200 µm. Such 3D microchannel networks are challenging to fabricate using soft lithography[17] or molding methods.[8,9,15,16] Figure 4b shows that upon hydraulic pressurization, all the pedals bend simultaneously with approximately the same bending angle to become closed (Figures S8,S9 and Movie S4, Supporting Information). It reopens upon withdrawing the fluid to mimic the bud-blossom process, which is well captured by the corresponding FEM simulation shown in Figure 4c.

In addition to unidirectional bending, localized bidirectional bending can also be achieved in a miniature single-channeled bending actuator to form an actuated wavy shape via direct multimaterial 3D printing. Figure 4d and Figure S10 (Supporting Information) show the schematic design with alternating patterning of SMP/elastomer segments on both top and bottom layers along the length. Pressurizing the single straight microfluidic channel leads to the alternate localized upward and downward bending in the patterned segments. Consequently, it generates a wavy configuration shown in the fully 3D-printed segmented bending actuator (Figure 4e; Figure S11 and Movie S5, Supporting Information) and corresponding FEM simulation (Figure 4f). Similar planar to wavy shape morphing is reported in thin composite strips when heated via direct 4D printing[41] Compared to thermal actuation, fluidic actuation facilitates fast and reversible actuation of programed shapes in simple control. Additionally, by alternately infusing fluid into mirrored microfluidic channels on both sides, a bidirectional bending MHSA is capable of bending to two opposing sides (Figures S12 and S13, Supporting Information).

2.5. Miniature Soft Hydraulic 3D Helical Actuators

When replacing the continuous stiff SMP layer with discrete oblique patterned SMP segments in the single-channel bending

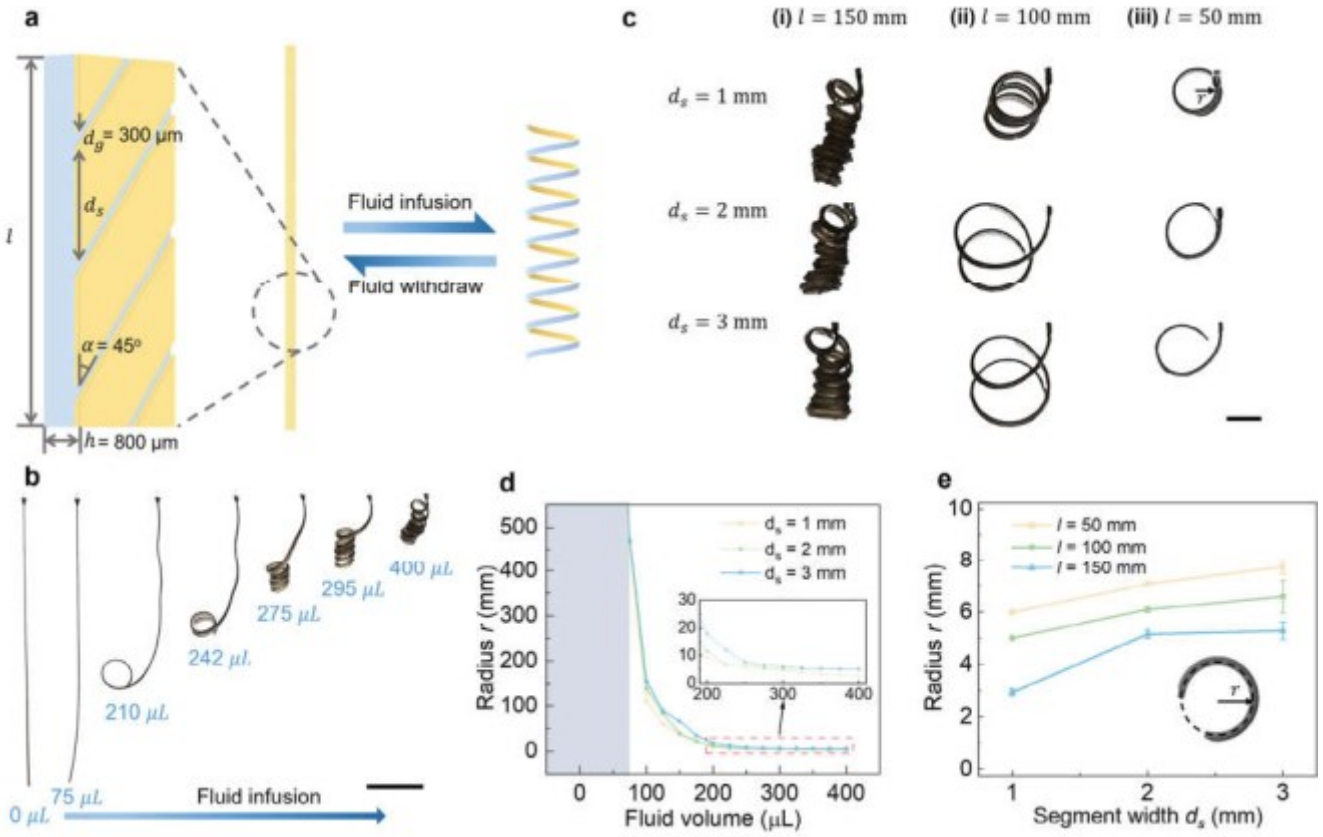

Figure 5. Miniature soft hydraulic 3D helical actuators. a) Schematic illustration of the 3D helical actuator with patterned discrete SMP segments. The segment width is d_s and the actuator length is l. It has gap width d_g = 300 μm, oblique angle 훼 = 45°, and width w = 3 mm. b) Snapshots of straight to coiling up process with the fluid infusion of 400 μL (l = 150 mm, d_s = 1 mm). Scale bar: 30 mm. c) Snapshots of the final coiled shapes in the helical actuators by tuning d_s and l. (l = 50 mm, V = 300 μL; l = 100 mm, V = 350 μL; l = 150 mm, V = 400 μL) Scale bar: 10 mm. d) Effect of d_s on the bending to coiling radius change as a function of V in the 3D helical actuators (l = 150 mm). e) Effect of l on the final coiling radius as a function of d_s in the 3D helical actuators.

actuator, it generates a 3D miniature helical actuator (Figure 5a; Figure S14, Supporting Information). Upon the increase of infused fluid volume, it morphs from a fully 3D printed long flat strip to a tightly coiled helix (Figure 5b; Movie S6, Supporting Information). The flat long oblique patterned strip can be characterized by the oblique angle 훼, the width d_s of the stiff SMP segments, the gap d_g between neighboring segments, and the strip length l. Without losing generality, we explore how l and d_s affect the actuated helical shapes by fixing 훼 = 45° and d_g = 300 μm (Figure 5c).

Figure 5b shows the actuated flat-to-coiling process upon increasing fluid volume from 0 to 400 μL. The actuator is 800 μm thick, 3 mm wide, and 150 mm long with d_s = 1 mm. The thickness of the stiff SMP layer segments is 100 μm and the microfluidic channel's cross-section size is 400 μm (width) × 200 μm (depth). Upon actuation, the free end bends first with a large bending radius R (R ≈450 mm at V = 75 μL, Figure 5d), and then twists and bends into one circle accompanied by a dramatically reduced radius (≈10 mm) at V = 210 μL, followed by quickly curling up into multiple loops at V = 242–295 μL. Finally, it contracts and tightens into a spiral spring-like shape without further shape changes, while only requiring a small V = 400 μL. Upon withdrawing the fluids, it returns to a straight strip. The tightly coiled helix has a small radius r of ≈3 mm and short length of ≈28.8 mm, which shrinks over five times compared to its original strip length. Similar actuated multi-loop spiral spring-like shapes are also observed in the long strips but with different d_s (Figure 5c(i)). As d_s increases, its actuated bending and coil-ing radii increase slightly (Figure 5d,e), while its final number of loops N reduces slightly (Figure 5c). However, reducing strip length l leads to a dramatic decrease in N and a moderate increase in the final coiling radius r due to the reduced flexibility. E.g., as l changes from 150 to 100 mm and to 50 mm at d_s = 2 mm, N reduces from 6 to 2 and to 1 with one single loop, respectively (Figure 5c), whereas r increases from ≈5 mm to ≈6 mm and to ≈7 mm, respectively (Figure 5e).

Similar shape morphing from planar ribbons to 3D helices is reported in both external stimuli-responsive hybrid soft-hard ribbons at small scales[10,52] and soft pneumatic filament actuators at macroscopic scale.[53,54] For the composite ribbons, the shape morphing is realized through discrete patterning of stiff inclusions within soft active materials in response to different external stimuli such as moisture, heat, and light,[10,52] while for the pneumatic actuators, it is realized through the inflation of an off-center axial channel in the soft filaments.[53,54] However, both methods often require multistep fabrication processes such

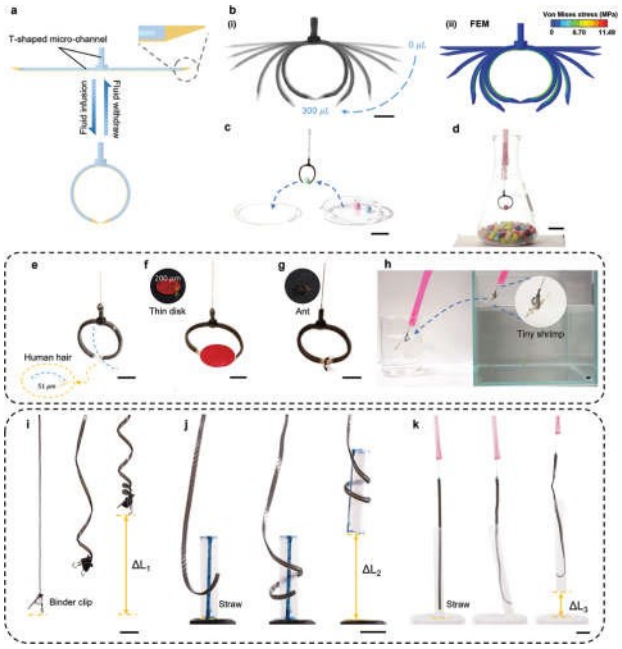

Figure 6. Applications in noninvasive manipulation and multi-modal entanglement grasping. a) Schematic design of a two-finger miniature soft gripper with 3D T-shaped microfluidic channel network and sharp tip ends. The two fingers can bend to form a closed circle for non-invasive and delicate manipulation. b) Snapshots of the closed-circle bending process of two fingers in the fully 3D printed actuator upon fluid infusion in experiments (i) and FEM simulation (ii). Scale bar = 5 mm. c,d) Demonstrations of transferring a small bead between two petri dishes (c) and grasping a bead from confined spaces such as a narrow-mouth Erlenmeyer flask (d). Scale bar = 15 mm. e–h) Demonstrations of delicate grasping of a human hair (diameter: 51 µm, e) and a thin disk (thickness: 200 µm, f) on flat surfaces, and non-invasive grasping of small fragile living organisms, such as a crawling ant (g) and a swimming tiny shrimp (h). Scale bar = 6 mm. i–k) Multi-modal manipulation in the tendril-like miniature soft hydraulic gripper in lifting a binder clip via artificial muscle mode (weight = 2.86 g, ΔL_1 = 80.8 mm, i), grasping a straw via external entangling (straw diameter: 12 mm and weight: 0.89 g, ΔL_2 = 48.9 mm, j) and internal entangling (straw diameter: 12 mm; weight: 0.44 g, ΔL_3 = 26.3 mm, k). Scale bar = 15 mm.

as sequential cross linking and developing in the composite[10,52] and dip coating and molding/demolding in pneumatic filament actuators,[53,54] in contrast to the directly printed miniature soft hydraulic actuators in a single print run.

2.6. Fully 3D Multi-Material-Printed Miniature Noninvasive Soft Hydraulic Grippers

Next, given the intrinsic benefits of miniature soft hydraulic actuators in small force (Figure 2h), small size, and fast response, we explore their potential applications as noninvasive and delicate grippers via direct multi-material printing.

Figure 6a,b(i) show the design and the fully 3D printed prototype of a simple T-shaped, two-finger miniature soft gripper, respectively (Figure S15, Supporting Information). It is composed of one vertical soft elastomer handle in the middle and two horizontal single-channel bending actuators. The actuator has a thickness of 800 µm and arm length of ≈18 mm. The gripper has a single interconnected 3D T-shaped microfluidic channel to drive the simultaneous bending of two fingers for grasping under a single hydraulic actuation input. To enhance the precise and delicate grasping of small-scale objects, we introduce a stiff wedge-shaped sharp tip to the fingertips with the tip thickness being 180 µm via direct multi-material printing without the need for additional assembly. Upon hydraulic infusion of 300 µL, the two fingers can bend into a half circle (i.e., 180° bending angle) with a bending radius of ≈5 mm, forming an approximate full circle with the two end tips almost aligning and contacting with each other, i.e., a close to 180° grasping angle when the two end tips meet (Movie S7, Supporting Information). The actuated bending process is well captured by the corresponding FEM simulation shown in Figure 6b(ii) and Movie S7 (Supporting Information).

The miniature two-finger gripper is delicate, precise, and gentle in handling both small-size deadweights and fragile living organisms (Movies S8 and S9, Supporting Information). We demonstrate that it can well-handle and manipulate small-size rigid beads (diameter of ≈4 mm) in both open spaces, e.g., transfer between petri dishes in Figure 6c, and confined spaces, e.g., picking up beads from a narrow-mouth Erlenmeyer flask in Figure 6d (Movie S8, Supporting Information). The large grasping angle (close to 180°) alongside the micro-scale thin tip also facilitates the precise and gentle grasping of small-scale and/or thin objects on flat surfaces (Movie S9, Supporting Information), such as a human hair with diameter of ≈51 µm (Figure 6e), a thin circular disk with thickness of 200 µm (Figure 6f), and a crawling tiny ant without any damage (Figure 6g). Furthermore, the miniature two-finger gripper can also be used under water for fast and noninvasive grasping of fragile living organisms, such as a tiny moving shrimp in a water tank. It can gently grasp and entangle around the tiny shrimp's soft body for safe transport and fast release in a water cup without any damage (Figure 6h; Movie S9, Supporting Information) due to its small force. We note that manipulating such small-scale or thin objects on flat surfaces and tiny living organisms under water in one single gripper is challenging for both miniature and macroscale soft grippers actuated by fluidic channels and other actuation methods. This is due to the tradeoff between compliance and precision, as well as the requirement of small contact areas between the grippers and small-scale objects during grasping and picking. The fully 3D printed two-finger gripper can be further extended to the design and direct printing of miniature three-finger grippers with three-branched microfluidic channels under single actuation input for more stable grasping, especially in handing the small beads shown in Figure S16 (Supporting Information).

2.7. Tendril-Like Multi-Modal Miniature Soft Manipulator

Based on the distinct curling and large contraction features in the miniature soft hydraulic 3D helical actuator discussed above, we further explore its potential applications as a tendril-like miniature soft gripper[55–57] for multimodal object manipulation.

Given the large contraction ratio of over 500% in the helical actuator, we first explore its application as artificial muscles. We show that the long helical strip actuator can lift a maximum of ≈2.86-gram dead weight, such as a binder clip, which is over five times its self-weight (0.55 gram), by means of coiling to contract

its length under the hydraulic actuation (Figure 6i; Movie S10, Supporting Information).

Furthermore, the long strip actuator is also capable of grasping a hollow cylindrical object, e.g., a straw with diameter of 12 mm, by two distinct means of tendril-like external entanglement[53,54] and internal entanglement. Different from picking and pinching, the entanglement involves adaptive and conformable contact interactions between the actuator and the grasped objects.[53,54] For external entanglement, upon actuation, the long strip first bends toward the straw, then it curls and wraps around the straw with multiple loops upon further actuation. Then, once the top loop contacts the straw, the free end loop quickly shrinks its radius to firmly wrap around and grasp the straw for lifting and manipulation (Figure 6j). For internal entanglement, the un-actuated miniature long straight strip actuator is first inserted deep into the small, confined space inside the straw (a diameter of 12 mm). As shown before in Figure 5d, upon actuation in free spaces without constraints, the free end of the long strip actuator will first bend into a large radius over 450 mm, which is over 30 times larger than the straw diameter. Thus, when placed inside the small tube, its actuated bending and coiling behavior will dramatically change since the confined space will significantly constrain its deformation. As shown in Figure 6k, the free end first bends to contact the inner wall with a dramatically reduced bending radius compared to the free space case, consequently, its loop coiling behavior is significantly suppressed. Upon further actuation, the strip becomes twisted along the length to create more contacts alongside the contact of the bended tip with the inner wall, anchoring itself to the tube for lifting. Such multimodal object manipulation complements the recently reported external entanglement grasping using an array of filament-like soft actuators.[54]

2.8. Integrating SME for Energy-Efficient Transportation and Programable Shape Morphing

Utilizing such temporary shape locking, we demonstrate its proof-of-concept application in energy-efficient miniature soft grippers by using two parallel bending actuators shown in Figure 7a. After bending to grasp the object, the soft gripper is heated above T_g (Figure 7a(ii)) using a remote IR emitter, followed by rapidly cooling to temporarily lock its grasped shape (Figure 7a(iii)). Thus, the grasped object can be held and transferred from disk 1 to disk 2 by the shape-locked bended gripper without consuming energy for transport. Furthermore, to release the grasped object, remotely reheating the temporarily locked shape above T_g leads to the recovery to its original permanent shape to release the object shown in Figure 3a(iv) and Figure 7a(iv).

Next, we further explore combining the designs of direct printing of microfluidic channel networks and the demonstrated SME for more complex and programable shape morphing and locking. As a proof-of-concept demonstration, we use two examples of 2D-to-3D shape morphing and locking to demonstrate the power of the fully 3D-printed strategy of miniature soft hydraulic actuators. Rather than the straight microfluidic channels demonstrated above, Figure 7b show a 3D mushroom-like miniature soft hydraulic actuator (Figure S17, Supporting Information) with a more complex curved microfluidic channel, e.g., a spiral concentric-shaped channel, and a connected straight vertical channel underneath, generating a 3D channel network under single actuation input. The disk has a radius of 15 mm and thickness of 1.1 mm with a 200 µm-thick SMP layer on its top. Infusing fluids into the spirally patterned channel leads to its shape morphing into a 3D saddle shape, which is well captured by the corresponding FEM simulation (Movie S11, Supporting Information). Similarly, the actuated and deformed saddle shape can be further temporarily locked by following the remote IR heating and rapid cooling process. Upon reheating, it recovers to its original flat shape. More complex microfluidic channel networks can be directly printed for programable 2D-to-3D shape morphing and locking. E.g., Figure 7c shows the design of a leaf-like miniature soft hydraulic actuator to mimic the warping process of leaves during growth (Figure S18, Supporting Information). The microfluidic channel network resembles the network of multi-branched midribs and veins in a real leaf. Upon the hydraulic pressurization, the leaf-like actuator deforms into a warping shape by bending along its long axis, which is well reproduced by the FEM simulation (Movie S11, Supporting Information). Similarly, its warped shape can be temporarily locked and recovered to its original flat shape by utilizing the SME.

3. Conclusion

We demonstrated fully 3D multi-material printed miniature soft hydraulic actuators with directly printed microfluidic channels and SME for shape morphing/locking and multimodal object manipulation. The soft actuators are directly printed in flat configurations for quickly and reversibly morphing into programed 2D and 3D shapes under hydraulic actuation. The shape morphing can be programed by spatially patterning either the stiff SMP layers/segments or the microfluidic channel networks for target shapes in 2D and 3D. Such programed shape changes can be temporarily locked by activating the SME of SMP components and recover to original shapes repeatedly. Benefitting from the small size, small force, fast response, and shape locking, the miniature hydraulic soft actuators have potential applications in non-invasive, precise, and/or multimodal manipulations of small-scale and/or thin objects and living organisms, as well as energy-saving manipulators.

High-resolution multi-material 3D printing alongside direct printing of microfluidic channels provides a powerful platform for creating fast-response, reversible, shape-morphing MSHAs with SME for shape locking and recovery in a simple yet controlled manner. It bridges the gap between the stimuli-responsive materials and the fluidic-driven soft actuators for programed shape morphing.[1,4,5] First, rich and complex 2D-to-3D shape morphing can be achieved in thin sheets of stimuli-responsive soft materials by programing anisotropic and/or inhomogeneous swelling/expansion/contraction in soft active materials and/or patterning of stiff inclusions,[10,11] while applying such shape-morphing strategies to soft fluidic actuators remains challenging due to the limitation in fabrication of both complex channel networks and patterned hybrid composites.[4] Third, once morphed, it is challenging to retain their morphed shapes upon removal of external stimuli or fluidic pressurization in most of the shape-morphing soft active materials and fluidic actuators due to their intrinsic reversible actuation responses.[1,10,11] In contrast,

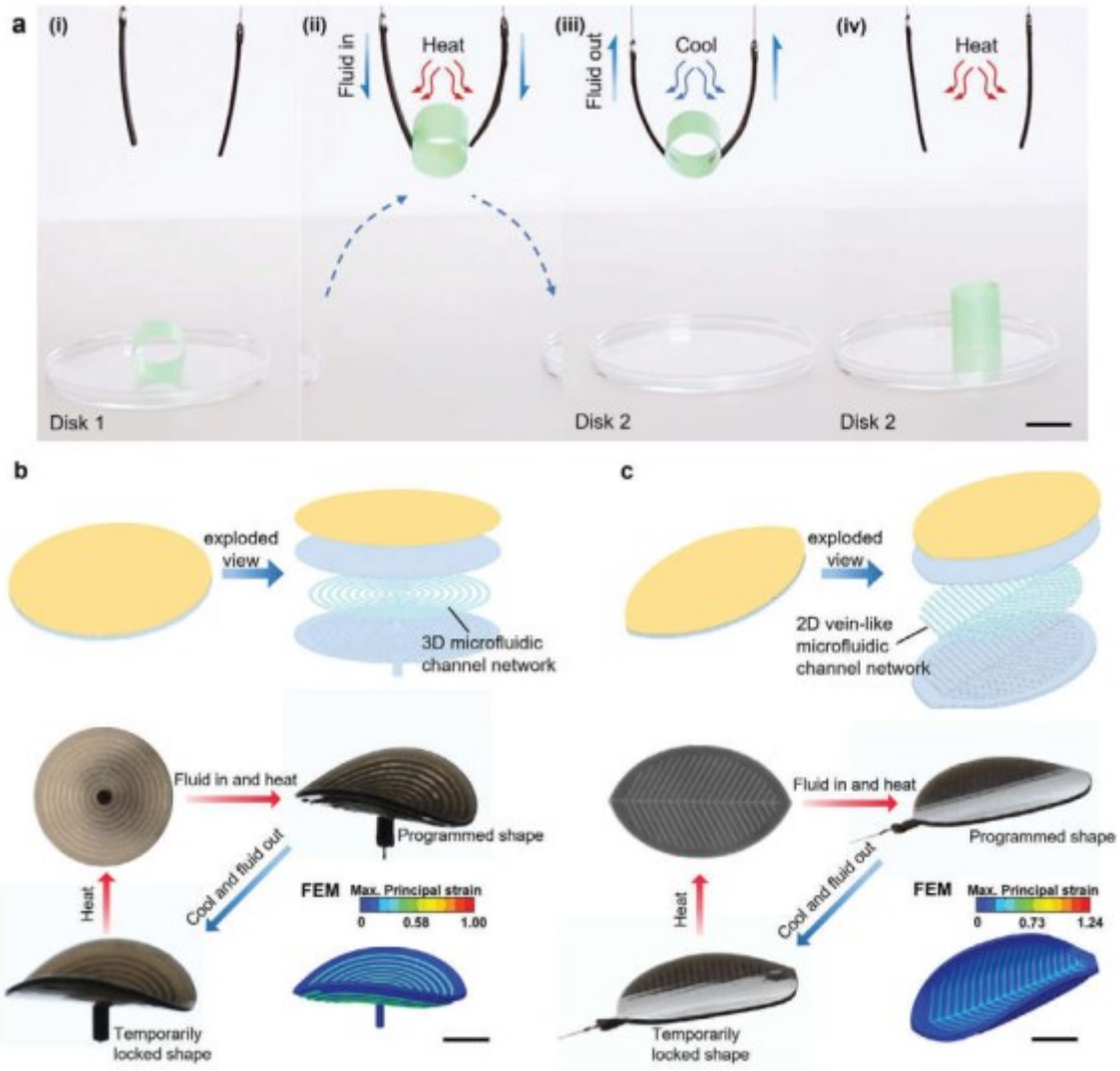

Figure 7. Shape morphing and locking in 3D printed miniature soft hydraulic actuators. a) Demonstration of the energy-efficient transportation process in a miniature soft gripper composed of two parallel bending actuators in handling a small tube. It utilizes the shape locking to hold and transport the grasped object without consuming energy (ii-iii) and the shape recovery to release the grasped object (iv). Scale bar = 10 mm. b,c) Demonstrated shape morphing, temporary locking, and recovery in two fully 3D printed thin mushroom-like (b) and thin leaf-like (c) miniature soft hydraulic actuators. The top row shows the schematic designs of the two actuators. The bottom row shows the experimental demonstration and FEM simulation results on their programed shape morphing into a saddle and warping shape, respectively. Scale bar = 10 mm.

the fully 3D-printed miniature hydraulic shape-morphing soft actuators integrate the benefits of both shape-morphing soft active materials and soft fluidic actuators. Combining direct printing of complex microfluidic channel networks and spatial multimaterial printing of patterned composites, it allows similar programed expansion anisotropy/inhomogeneity and patterned hybrids to soft active thin sheets and beyond. This is achieved in a more controllable manner for rich and fast shape morphing, as well as temporary shape locking by activating the SME in the printed SMP compositions.

Despite the promising results in this study, we note there are several limitations of this work. First, the durability of the directly 3D-printed miniaturized soft hydraulic actuators needs to be further improved. It shows a rather limited fatigue life of from tens to over a hundred cycles of actuation and de-actuation before bursting, depending on the range of bending angles (Figure S19, Supporting Information). The fatigue life could be potentially improved by optimizing the geometric designs of the actuators, such as the microfluidic channel size, channel patterns, and the bilayer thickness ratios, and enhancing the toughness and flexibility of soft digital elastomeric materials, as well as integrating reinforcement structures such as fiber-reinforced sheath. Second, the lifespan of the 3D-printed miniature soft actuators is limited to a short period of time (several weeks) due to the environment-impacted degradation of the 3D-printed materials. The degradation of the 3D printed materials could be minimized by post-processing treatments such as coatings or surface treatments to enhance the resistance.

4. Experimental Section

Sample Design and 3D Printing: The individual parts of the samples were printed on a commercial 3D multi-material printer (Objet 260 Connex 3, Stratasys), with a 30 μm resolution under digital print-ing mode. Commercial materials Agilus 30 Black was used as the soft elastomer, VeroWhite as the stiff SMP, SUP 706B as the support mate-rial for 3D printing, and cleaning fluid as the non-curing support mate-rial for building the microfluidic channels. All materials were purchased from Stratasys (Eden Prairie, MN, USA). After 3D printing, samples were immersed in an ultrasonication bath to remove the SUP 706B support material.

Characterization of SMP: To characterize the thermomechanical properties of the SMP materials, dynamic mechanical analysis (DMA) and differential scanning calorimetry (DSC) were performed (DMA850 and Q100, TA Instruments, New Castle, DE, USA). To test the thermomechanical properties of the SMP material, they were placed in the DMA in tension mode and cycled at 1 Hz and cycled from 30 to 90 °C. DSC was carried out on a model Q100, DSC tester. Samples (≈5 mg) were contained in aluminum pans and subjected to thermal cycles from −40 to 150 °C at a ramp rate of 10 °C/min.

Characterization of Miniature Soft Actuator Deformation: To characterize the bending deformation of the soft actuator as a function of the fluid volume, the blocking force (blocked at 0°) was recorded by an Instron (Instron 5944, Norwood, MA, USA) while the fluid was infused by a Syringe pump (Harvard Apparatus, Holliston, MA) from 0 to 200 μL in 30 s. The actuators were clamped on the syringe pump horizontally and placed under the load cell, and the tips of the actuator contact with an indenter which was clamped in the jaws of the Instron. The fluid then infused continuously into the actuators and the resulting vertical blocking force was measured, as shown in Figure 2h.

FEM Simulation: FEM simulations were performed in Abaqus/Standard (Dassault Systèmes) to simulate the shape change of the fully 3D-printed miniature soft hydraulic actuators. The geometry of all actuators was imported into Abaqus CAE as a step file and meshed with solid quadratic tetrahedral elements (C3D10H). A mesh refinement study was applied to verify the accuracy of the mesh. Both VeroWhite (strain limited layer) and AgilusBlack (soft elastomer layer embedded with microfluidic channels) were modeled as linear elastic models with Young's Modulus $E_{VeroWhite}$ = 1.024 GPa, $E_{AgilusBlack}$ = 0.455 MPa and Poisson's ratio $\nu_{VeroWhite}$ = 0.33, $\nu_{AgilusBlack}$ = 0.40, respectively. Static simulation performed as pressure was applied to inner cavities for fluid-driven inflation.

Temporarily Shape Locking and Shape Recovery: A 250-Watt Ceramic IR emitter (Diameter: 12.5 cm) was used to heat the 3D-printed soft actuators above the glass transition temperature (T_g) of the SMP. The distance between the IR emitter and soft actuators at 120 mm for 5 seconds in every heating process, was maintained. For rapid cooling process, an open-air cooler was used to rapidly reduce the temperature of the SMP below T_g, temporarily locking the deformed shape of the soft actuators. In the shape recovery process, the IR emitter was used to heat the SMP of the soft actuators above T_g, gradually recovering the soft actuators to their original permanent shapes.

Supporting Information

Supporting Information is available from the Wiley Online Library or from the author.

Acknowledgements

The authors thank the help from Ms. F. Krisnadi in Dr. M. D. Dickey's lab with the DSC measurements. J.Y. acknowledges the funding support from the National Science Foundation under award number CMMI-2126072 and 2329674.

Conflict of Interest

The authors declare no conflict of interest.

Author Contributions

H.Q. and Y.C. contributed equally to this work. H.Q. Y.C., and J.Y. developed the concept and designed the experiments. H.Q. and Y.C. fabricated and characterized the prototypes. H.Q. Y.C., and Y.Z. conducted the experiments. Y.C. conducted the finite element analysis simulations. Y.H. conducted the theoretical model. H.Q. drafted the manuscript. J.Y. revised the manuscript. All the authors contributed to the discussion, data analysis, and editing of the final manuscript.

Data Availability Statement

The data that support the findings of this study are available in the supporting information of this article.

Keywords

3D printing, miniature soft fluidic actuator, non-invasive and delicate grasping, shape locking, shape memory effect, shape morphing

Received: February 18, 2024
Revised: May 16, 2024
Published online:

[1] L. Hines, K. Petersen, G. Z. Lum, M. Sitti, Adv. Mater. 2017, 29, 1603483.
[2] M. Sitti, Nat. Rev. Mater. 2018, 3, 74.
[3] C. S. X. Ng, M. W. M. Tan, C. Xu, Z. Yang, P. S. Lee, G. Z. Lum, Adv. Mater. 2021, 33, 2003558.
[4] Y. Chi, Y. Zhao, Y. Hong, Y. Li, J. Yin, Advanced Intelligent Systems 2023, 6, 2300063.
[5] Y. Chi, Y. Li, Y. Zhao, Y. Hong, Y. Tang, J. Yin, Adv. Mater. 2022, 34, 2110384.
[6] Z. Shen, F. Chen, X. Zhu, K.-T. Yong, G. Gu, J. Mater. Chem. B 2020, 8, 8972.
[7] Y. Zhao, M. Hua, Y. Yan, S. Wu, Y. Alsaid, X. He, Annu. Rev. Control Robot. Auton. Syst. 2022, 5, 515.
[8] J. Walker, et al., in Actuators 3 (MDPI).
[9] M. S. Xavier, C. D. Tawk, A. Zolfagharian, J. Pinskier, D. Howard, T. Young, J. Lai, S. M. Harrison, Y. K. Yong, M. Bodaghi, A. J. Fleming, IEEE Access 2022, 10, 59442.
[10] S.-J. Jeon, A. W. Hauser, R. C. Hayward, Acc. Chem. Res. 2017, 50, 161.
[11] D. Jiao, Q. L. Zhu, C. Y. Li, Q. Zheng, Z. L. Wu, Acc. Chem. Res. 2022, 55, 1533.
[12] H. Kim, S.-K. Ahn, D. M. Mackie, J. Kwon, S. H. Kim, C. Choi, Y. H. Moon, H. B. Lee, S. H. Ko, Mater. Today 2020, 41, 243.
[13] T. van Manen, S. Janbaz, A. A. Zadpoor, Mater. Today 2018, 21, 144.
[14] A. Nojoomi, J. Jeon, K. Yum, Nat. Commun. 2021, 12, 603.
[15] B. Mosadegh, P. Polygerinos, C. Keplinger, S. Wennstedt, R. F. Shepherd, U. Gupta, J. Shim, K. Bertoldi, C. J. Walsh, G. M. Whitesides, Adv. Funct. Mater. 2014, 24, 2163.
[16] E. Siéfert, E. Reyssat, J. Bico, B. Roman, Nat. Mater. 2019, 18, 24.
[17] T. Ranzani, S. Russo, N. W. Bartlett, M. Wehner, R. J. Wood, Adv. Mater. 2018, 30, 1802739.
[18] M. Wehner, R. L. Truby, D. J. Fitzgerald, B. Mosadegh, G. M. Whitesides, J. A. Lewis, R. J. Wood, Nature 2016, 536, 451.

[19] Y.-F. Zhang, C. J.-X. Ng, Z. Chen, W. Zhang, S. Panjwani, K. Kowsari, H. Y. Yang, Q. Ge, Adv. Mater. Technol. 2019, 4, 1900427.
[20] A. T. Alsharhan, O. M. Young, X. Xu, A. J. Stair, R. D. Sochol, J. Micromech. Microeng. 2021, 31, 044001.
[21] H. Meng, G. Li, Polymer 2013, 54, 2199.
[22] Q. Zhao, H. J. Qi, T. Xie, Prog. Polym. Sci. 2015, 49, 79.
[23] E. C. Davidson, A. Kotikian, S. Li, J. Aizenberg, J. A. Lewis, Adv. Mater. 2020, 32, 1905682.
[24] M. Bobnar, N. Derets, S. Umerova, V. Domenici, N. Novak, M. Lavric, G. Cordoyiannis, B. Zalar, A. Resetic, Nat. Commun. 2023, 14, 764.
[25] Q. Ze, X. Kuang, S. Wu, J. Wong, S. M. Montgomery, R. Zhang, J. M. Kovitz, F. Yang, H. J. Qi, R. Zhao, Adv. Mater. 2020, 32, 1906657.
[26] R. MacCurdy, R. Katzschmann, K. Youbin, D. Rus, in 2016 IEEE International Conference on Robotics and Automation (ICRA), 3878.
[27] N. P. Macdonald, J. M. Cabot, P. Smejkal, R. M. Guijt, B. Paull, M. C. Breadmore, Anal. Chem. 2017, 89, 3858.
[28] Y. Chi, Y. Tang, H. Liu, J. Yin, Adv. Mater. Technol. 2020, 5, 2000370.
[29] S. P. Timoshenko, J. M. Gere, Theory of elastic stability, Dover Publications, Mineola, New York, 2009.
[30] G. Alici, T. Canty, R. Mutlu, W. Hu, V. Sencadas, Soft Rob. 2018, 5, 24.
[31] I. C. Christov, V. Cognet, T. C. Shidhore, H. A. Stone, J. Fluid Mech. 2018, 841, 267.
[32] Y. Hong, Y. Zhao, J. Berman, Y. Chi, Y. Li, H. Huang, J. Yin, Nat. Commun. 2023, 14, 4625.
[33] N. R. Sinatra, C. B. Teeple, D. M. Vogt, K. K. Parker, D. F. Gruber, R. J. Wood, Sci. Rob. 2019, 4, eaax5425.
[34] W. Wang, C. Li, M. Cho, S.-H. Ahn, ACS Appl. Mater. Interfaces 2018, 10, 10419.
[35] Y.-F. Zhang, N. Zhang, H. Hingorani, N. Ding, D. Wang, C. Yuan, B. Zhang, G. Gu, Qi. Ge, Adv. Funct. Mater. 2019, 29, 1806698.
[36] D. J. Roach, X. Sun, X. Peng, F. Demoly, K. Zhou, H. J. Qi, Adv. Funct. Mater. 2022, 32, 2203236.
[37] H. T. Lee, F. Seichepine, G. Z. Yang, Adv. Funct. Mater. 2020, 30, 2002510.
[38] R. L. Truby, M. Wehner, A. K. Grosskopf, D. M. Vogt, S. G. M. Uzel, R. J. Wood, J. A. Lewis, Adv. Mater. 2018, 30, 1706383.
[39] B. Gorissen, W. Vincentie, F. Al-Bender, D. Reynaerts, M. De Volder, J. Micromech. Microeng. 2013, 23, 045012.
[40] C. B. Teeple, T. N. Koutros, M. A. Graule, R. J. Wood, Int. J. Rob. Res. 2020, 39, 1647.
[41] Z. Ding, C. Yuan, X. Peng, T. Wang, H. J. Qi, M. L. Dunn, Sci. Adv. 2017, 3, 1602890.
[42] J. Paek, I. Cho, J. Kim, Sci. Rep. 2015, 5, 10768.
[43] W. Wang, C. Y. Yu, A. Serrano, A. P., S.-H. Ahn, Soft Rob. 2020, 7, 283.
[44] G. Mao, M. Drack, M. Karami-Mosammam, D. Wirthl, T. Stockinger, R. Schwödiauer, M. Kaltenbrunner, Sci. Adv. 2020, 6, eabc0251.
[45] J. Sun, E. Lerner, B. Tighe, C. Middlemist, J. Zhao, Nat. Commun. 2023, 14, 6023.
[46] Y. Zhang, C. Pan, P. Liu, L. Peng, Z. Liu, Y. Li, Q. Wang, T. Wu, Z. Li, C. Majidi, L. Jiang, Nat. Commun. 2023, 14, 4428.
[47] T. N. Do, H. Phan, T. Q. Nguyen, Y. Visell, Adv. Funct. Mater. 2018, 28, 1800244.
[48] A. Leber, C. Dong, S. Laperrousaz, H. Banerjee, M. E. M. K. Abdelaziz, N. Bartolomei, B. Schyrr, B. Temelkuran, F. Sorin, Adv. Sci. 2023, 10, 2204016.
[49] Y. Cui, X.-J. Liu, X. Dong, J. Zhou, H. Zhao, IEEE Trans. Robot. 2021, 37, 1604.
[50] S. Abondance, C. B. Teeple, R. J. Wood, IEEE Robot. Autom. Lett. 2020, 5, 5502.
[51] B. Fang, F. Sun, L. Wu, F. Liu, X. Wang, H. Huang, W. Huang, H. Liu, L. Wen, Soft Rob. 2022, 9, 233.
[52] Z. L. Wu, M. Moshe, J. Greener, H. Therien-Aubin, Z. Nie, E. Sharon, E. Kumacheva, Nat. Commun. 2013, 4, 1586.
[53] T. J. Jones, E. Jambon-Puillet, J. Marthelot, P.-T. Brun, Nature 2021, 599, 229.
[54] K. Becker, C. Teeple, N. Charles, Y. Jung, D. Baum, J. C. Weaver, L. Mahadevan, R. Wood, Proc. Natl. Acad. Sci. U. S. A. 2022, 119, 2209819119.
[55] S. J. Gerbode, J. R. Puzey, A. G. McCormick, L. Mahadevan, Science 2012, 337, 1087.
[56] H. Lu, M. Zhang, Y. Yang, Q. Huang, T. Fukuda, Z. Wang, Y. Shen, Nat. Commun. 2018, 9, 3944.
[57] I. Must, E. Sinibaldi, B. Mazzolai, Nat. Commun. 2019, 10, 344.